EFFECT OF GLASS-BATCH MAKEUP ON THE MELTING PROCESS

PAVEL HRMA, MICHAEL J. SCHWEIGER, CARISSA J. HUMRICKHOUSE, J. ADAM MOODY,
RACHEL M. TATE, TIMOTHY T. RAINSDON, NATHAN E. TEGROTENHUIS,
BENJAMIN M. ARRIGONI, JOSÉ MARCIAL, CARMEN P. RODRIGUEZ, BENJAMIN H. TINCHER

Pacific Northwest National Laboratory, Richland, Washington, USA

E-mail: pavel.hrma@pnl.gov

Submitted February 26, 2010; accepted May 11, 2010

Keywords: Glass batch makeup, Glass batch melting, Nuclear waste glass, Glass foaming

The response of a glass batch to heating is determined by the batch makeup and in turn determines the rate of melting. Batches formulated for a high-alumina nuclear waste to be vitrified in an all-electric melter were heated at a constant temperature-increase rate to determine changes in melting behavior in response to the selection of batch chemicals and silica grain-size as well as the addition of heat-generating reactants. The type of batch materials and the size of silica grains determine how much, if any, primary foam occurs during melting. Small quartz grains, 5 μm in size, caused extensive foaming because their major portion dissolved at temperatures <800°C, contributing to the formation of viscous glass-forming melt that trapped evolving batch gases. Primary foam did not occur in batches with larger quartz grains, ±75 μm in size, because their major portion dissolved at temperatures >800°C when batch gases no longer evolved. The exothermal reaction of nitrates with sucrose was ignited at a temperature as low as 160°C and caused a temporary jump in temperature of several hundred degrees. Secondary foam, the source of which is oxygen from redox reactions, occurred in all batches of a limited composition variation involving five oxides, B_2O_3, CaO, Li_2O, MgO, and Na_2O. The foam volume at the maximum volume-increase rate was a weak function of temperature and melt basicity. Neither the batch makeup nor the change in glass composition had a significant impact on the dissolution of silica grains. The impacts of primary foam generation on glass homogeneity and the rate of melting in large-scale continuous furnaces have yet to be established via mathematical modeling and melter experiments.

INTRODUCTION

The rate of heat-transfer from molten glass to the batch blanket and the kinetics of various chemical reactions and phase transitions jointly control the batch-to-glass conversion process in a continuous glass melter [1–3]. With an increasingly effective heat transfer in advanced melters, the kinetics of reactions within the batch blanket becomes more prominent as the rate-controlling process. Thus, the makeup of the batch, i.e., the selection and pretreatment of the batch materials, becomes more important for melting efficiency.

This study was undertaken to understand the relationship between the glass-batch makeup and the response of the batch to heating. One of the responses of a batch to heating is the formation of foam [4-10]. Gerrard and Smith [4] recognize two types of foam, primary foam, i.e., the expansion of the batch by evolving batch gases trapped in the glass-forming melt, and secondary foam produced in molten glass as an accumulation of fining bubbles.

Another response frequently studied is the process whereby batch solids in the glass-forming melt dissolve and finally disappear as the melting process is completed [11-19].

However, there is much more to melting behavior than volume expansion and solid-phase dissolution. A glass batch is a mixture of two groups of materials. Oxides, acids, hydroxides, and oxyhydrates, such as silica, silicates, boric acid, iron oxide and hydroxide, alumina, etc., are in one group. Ionic salts, such as carbonates, nitrates, sulfates, halides, etc., are in the other. On heating the batch, multiple processes take place [1-3, 20-28], partly simultaneously and partly successively:

1) water evaporation,
2) elimination of chemically bonded water (crystalline water, water from hydroxides and oxyhydrates, and water from boric acid),
3) melting of oxyionic salts,
4) molten salt migration,
5) formation of borate melt,
6) reactions of this melt with molten salts and with amorphous Fe_2O_3 and Al_2O_3 from $Fe(OH)_3$ and $Al(OH)_3$,
7) formation of intermediate crystalline phases (e.g., spinel in nuclear waste glasses),
8) reaction of nitrates with organics,
9) reaction of molten salts with solid silica,

10) formation of a continuous glass-forming melt,
11) volatilization, expansion, and collapse of primary foam,
12) dissolution of residual solids (mainly silica).

To simplify the matter, we may separate these processes in two major stages: Stage I, during which batch gases can freely escape through open pores, and Stage II, at which the pores are closed and the batch is converted into a mixture of glass-forming melt, solid residues, and gas bubbles.

In glasses with multiple redox components, such as waste glasses containing Mn_2O_3, Fe_2O_3, and CrO_3, there is a smooth transition from the evolution of batch gases (H_2O, CO_x, NO_x, N_2, and O_2) to the evolution of O_2 from redox reactions (this O_2 can be classified as fining gas), and thus primary foam and secondary foam are not two distinct foaming events. However, because the evolution of batch gases is complete at a temperature that generally does not exceed 800°C, we can expect the formation of primary foam only when the formation of continuous glass-forming melt occurs below 800°C. Primary foam and secondary foam occur at different temperature intervals in commercial glasses with sodium sulfate as a fining agent [9,29].

This study was performed with batches formulated for vitrifying nuclear materials. Batches were made for glasses designed to immobilize high-alumina high-level waste. As in our previous studies [30-32], we prepared a batch marked A0 from materials closely resembling the mineral composition of the actual high-level waste and additives specifically selected for easy melting. The glass formulation for A0 came from Vitreous State Laboratory (VSL) and was previously produced at VSL in a continuous all-electric melter equipped with bubblers from a batch made from different mineral components. The main difference was in the mineral form of alumina, which was gibbsite, $Al(OH)_3$, in the A0 batch, and crystalline Al_2O_3 (corundum) in the VSL batch.

Several series of experiments are reported in this paper. In the first series, we measured the expansion of the A0 batch resulting from a gradual increase of temperature and compared it with the expansion of a batch prepared at VSL (in this study called Al-Na batch) for a glass of a similar composition. We have also measured by X-ray diffraction (XRD) the content of solid silica in these batches during increasing temperature. Additionally, we investigated the evolution of the temperature field in a larger volume of a heated A0 batch. Some of these results were published previously [31, 32].

In the second and third series, we varied silica-grain size and added sucrose to the nitrated A0 batch. Finally, in the forth series of experiments, we varied the composition of A0 glass without changing the composition and content of its high-level waste portion. Five additive components were varied: B_2O_3, CaO, Li_2O, Na_2O, and MgO.

The results of this study are discussed in terms of understanding the melting process in general and with regard to the melting behavior in the batch blanket in a continuous electric melter in particular.

EXPERIMENTAL

Table 1 presents the compositions of Al-Na glass and A0 glass. Both of these glasses were formulated at the VSL as Al-Na-limited high-level waste glass and Al-limited high-level waste glass (denoted here as Al-Na and A0, respectively, for simplicity). A0 glass contains 45 mass% of the waste components (see Ref. [30] for details).

Table 2 presents the corresponding batch compositions. The Al-Na batch was formulated and prepared at VSL. The A0 batch was designed for this study using chemicals that simulate the actual waste as truly as possible and easy-reacting additives, e.g., hydroxides instead of oxides, or Na_2CrO_4 instead of Cr_2O_3.

Table 1. Glass compositions in mass fractions.

	Al–Na	A0		Al–Na	A0
Al_2O_3	0.2134	0.2400	MgO	0.0022	0.0012
B_2O_3	0.1836	0.1521	Na_2O	0.1271	0.0959
BaO	0.0003	0.0000	NiO	0.0010	0.0040
Bi_2O_3	0.0116	0.0114	P_2O_5	0.0202	0.0105
CaO	0.0072	0.0609	PbO	0.0009	0.0041
CdO	0.0001	0.0000	SiO_2	0.3457	0.3051
Cr_2O_3	0.0071	0.0052	SO_3	0.0022	0.0020
F	0.0023	0.0067	TiO_2	0.0017	0.0000
Fe_2O_3	0.0281	0.0591	ZnO	0.0018	0.0008
K_2O	0.0066	0.0014	ZrO_2	0.0012	0.0039
Li_2O	0.0357	0.0357			

Table 2. Batch compositions in kg of precursors per kg of glass.

	Al–Na	A0		Al–Na	A0
Al_2O_3	0.2134		$Ni(OH)_2$	0.0012	–
$Al(OH)_3$	–	0.3675	$NiCO_3$	–	0.0064
H_3BO_3	0.3262	0.2698	$FePO_4$	0.0429	–
$BaCO_3$	0.0004	–	$Fe(H_2PO_2)_3$	–	0.0124
Bi_2O_3	0.0116	–	PbO	0.0009	–
$Bi(OH)_3$	–	0.0128	$Pb(NO_3)_2$	–	0.0061
CaO	0.0072	0.0608	SiO_2	0.3457	0.3051
CdO	0.0001	–	Na_2SO_4	0.0038	0.0036
Cr_2O_3	0.0071	–	TiO_2	0.0017	–
Na_2CrO_4	–	0.0111	ZnO	0.0018	–
NaF	0.0050	0.0148	$Zn(NO_3)_2{\cdot}4H_2O$	–	0.0027
$Fe(OH)_3$	0.0072	0.0738	$Zr(OH)_4$	0.0016	–
KNO_3	0.0142	0.0030	$Zr(OH)_4{\cdot}0.65H_2O$	–	0.0055
Li_2CO_3	0.0884	0.0883	Na_2CO_3	0.0212	–
MgO	0.0022	–	$NaNO_2$	0.0150	0.0034
$Mg(OH)_2$	–	0.0017	$NaNO_3$	0.0548	0.0049
NaOH	0.1066	0.0971	$Na_2C_2O_4{\cdot}3H_2O$	–	0.0018
			Sum	*1.2802*	*1.3526*

Five variations of A0 glass were produced by changing fractions of B_2O_3, CaO, Li_2O, Na_2O, and MgO (see Table 3) while keeping the waste composition the same as in A0 batch and the mass fraction of waste components in glass at the fixed level of 0.45.

Table 3. Batch composition variation in kg of precursors per kg of glass. Additions of all other precursors were the same as in Table 2.

	A0	A1	A2	A3	A4	A5
CaO	0.0608	0.0458	0.0608	0.1008	0.0608	0.0358
H_3BO_3	0.2698	0.2965	0.2698	0.1988	0.2130	0.2698
Li_2CO_3	0.0883	0.0883	0.1674	0.0883	0.1674	0.1194
$Mg(OH)_2$	0.0017	0.0017	0.0017	0.0017	0.0017	0.0379
NaOH	0.0971	0.0971	0.0558	0.0971	0.0971	0.0809

The silica-grain size was varied in the A0 batch. While all batches used in this study were prepared with silica flour of ≤ 75 mm grain–size, additional two batches were prepared with fine silica (≤ 5 mm) and with large-grain sand (350 to 850 mm, 550 mm on average).

To study the effect of an internal heat source, we added cellulose or sucrose to an A0 batch acidified with HNO_3 to pH 1.

All batches were prepared in the form of slurry that was subsequently dried. More detailed description of batch preparation is given in Ref. [32].

Various methods of testing and analysis are available to examine the response of a batch to heating, i.e., for identifying and quantifying the main batch reactions. In this work, we used thermal gravimetric analysis (TGA), X-ray diffraction (XRD), scanning electron microscopy-energy-dispersive spectroscopy (SEM-EDS), and optical microscopy (see Ref. [32] for details).

Batches were heated at 5°C/min, and the conversion process was recorded as a function of temperature.

We used two methods for the volume changes of batches during heating. In one, loose dry batches, 21.8 g, were heated at 5°C/min in cylindrical silica-glass crucibles, 46 mm in diameter. In the other, cylindrical pellets, 13 mm in diameter and 6 mm high, were prepared from 1.50 g of batch pressed at 7 MPa. Pellets were heated at 5°C/min on an alumina plate. Both loose batches and pellets were photographed through a window in the furnace wall. The images were evaluated in Photoshop® to obtain the batch height in crucibles and profile areas of pellets.

Batch samples, 10 g, were heated in porcelain or platinum crucibles to various temperatures and quenched. Thin sections were prepared from these samples for optical and electron microscopy and powders with 5 wt.% CaF_2 as a reference standard for XRD.

The temperature-field evolution was measured in large silica crucibles (200 mm tall and 135 mm in diameter) equipped with a battery of thermocouples [30,31].

We postponed the application of other methods, such as differential scanning calorimetry and evolved gas analysis to future experiments. However, we attempted the flux migration test [33], a technique designed to estimate the extent at which molten salts are likely to migrate within and possibly out of the batch blanket, but stopped using it since there was no evidence of salt migration after testing two batches.

RESULTS

Melting of loose batches

Figure 1 displays the expansion of loose batches in silica-glass crucibles in response to heating at 5°C/min. The loose A0 batch began to expand at ~800°C, i.e., when the batch reactions were complete, thus producing mild secondary foam that reached a maximum relative expansion of 1.64 (measured as the increase in the sample relative height, h/h_0, where h is the sample average height and the subscript 0 stands for the initial value). Because loose batches were placed in cylindrical quartz-glass crucibles, their relative height equals their relative volume, $v = V/V_0$, where V is the total volume. The loose Al-Na batch began to expand at ~730°C and reached a maximum relative expansion of 5.42 at 900°C. Thus, the expansion of the loose Al-Na batch began as primary foam that turned to secondary foam as the temperature rose above 800°C.

The foam density can be estimated based on the mass and volume of samples. The initial density of the loose Al-Na batch was ~0.97 g/cm^3. At 650°C, the density increased, as a result of sintering, to a maximum value of 1.07 g/cm^3. During the following expansion, the density of primary foam decreased to a value as low as ~0.26 g/cm^3 at 800°C. At this point, foam contained 7.6 vol% of melt. The density of secondary foam decreased to a value ~0.18 g/cm^3 at 900°C, containing

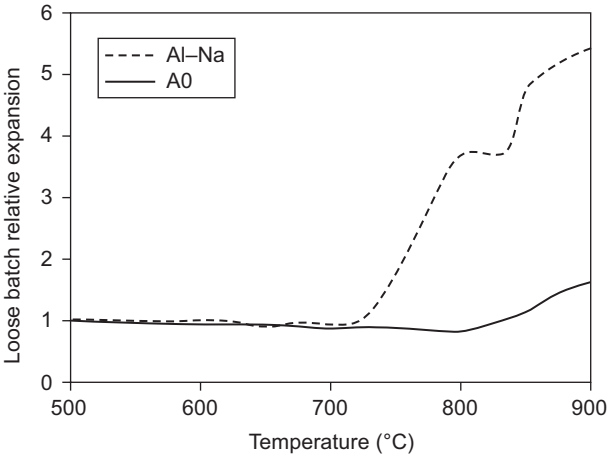

Figure 1. Relative batch height versus temperature for Al-Na and A0 batches placed in silica-glass crucible and heated at 5°C/min.

5.2 vol% of melt. With such a high gas-phase fraction, foam was collapsing through the coalescence of cells rather than by film drainage [35]. The cells coalesced into large cavities that burst, leading to a sudden decrease in volume. An example of such cavities is seen in Figure 2 (note that the cavities considerably shrank during cooling).

Figure 3 shows the mass change by TGA of the batches heated at 5°C/min. The mass ratio is defined as $m_R = (m_T - m_G)/(m_0 - m_G)$, where m_0 is the initial mass, m_T is the sample mass at temperature T, and m_G is the final mass (the glass mass). The major mass loss began at ~150°C, continued first at a fast rate to 600°C for the Al-Na batch and to 650°C for the A0 batch, and then continued at a slow rate from 600°C to ~800°C; the mass loss above 800°C was barely measurable.

As Figure 3 indicates, there is little difference between mass losses, i.e., gas evolution, of the two batches at temperatures above 700°C. Therefore, the most likely cause of the difference in foam formation between Al-Na and A0 batches is the difference of the temperature at which the glass-forming phase became continuous, and the open pores closed.

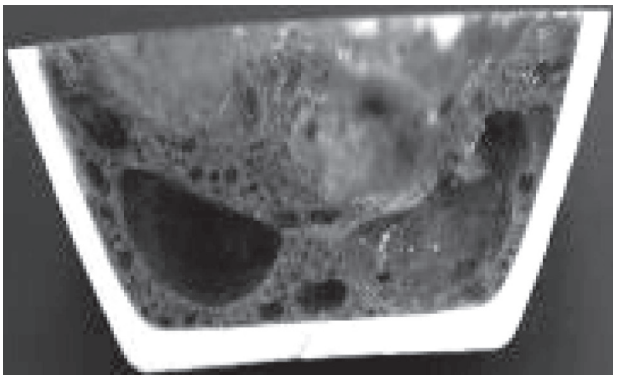

Figure 2. Cross-section of Al-Na sample heated at 5°C/min to 800°C and quenched. The diameter of the bottom of the porcelain crucible is 22 mm.

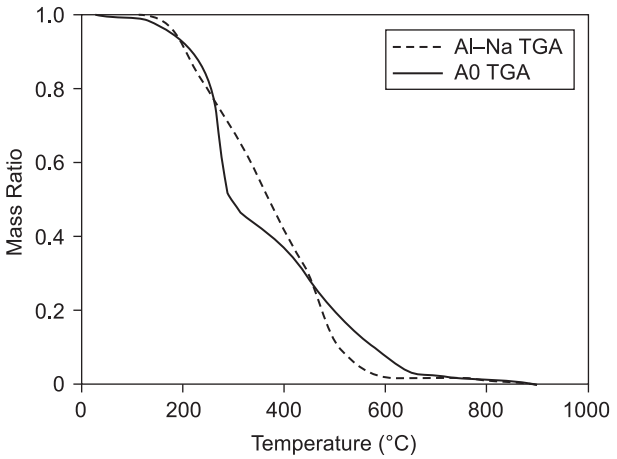

Figure 3. Mass of Al-Na batch per mass of glass as a function of temperature during 5°C/min heating by TGA.

One can assume that the glass-forming melt becomes continuous by surface forces as soon as the viscosity becomes low enough to enable the melt to flow at a high enough velocity. This viscosity can be assessed as $\eta \approx \sigma/u$, where η is the viscosity, σ is the surface tension, and u is the velocity. Since for borosilicate glasses, σ is ~ 0.3 kg/s^2, then a pore of 2 mm in radius will close within 1 s at a viscosity of ~150 Pa·s.

As seen from Figure 4, Al-Na and A0 glasses have virtually identical viscosities. Based on a viscosity-composition relationship [35], the Al-Na glass has a viscosity of 150 Pa·s at 863°C and the A0 glass at 857°C. However, foam occurred in Al-Na and A0 glasses at a lower temperature and in Al-Na glass at a temperature ~80°C lower than in A0 glass. To explain these differences, we need to consider the structure of the melts on the silica grain-size scale and the differences in the makeup of the batches.

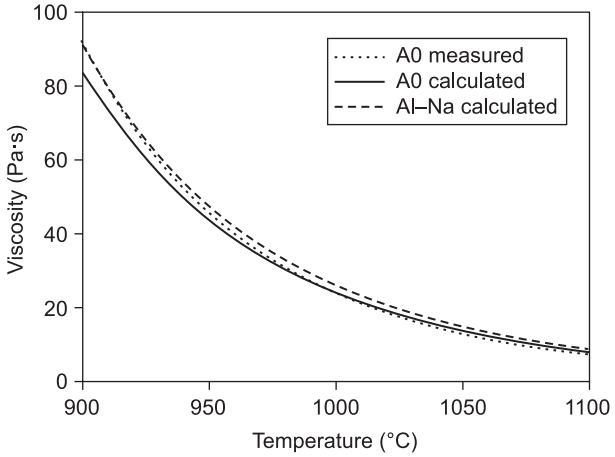

Figure 4. Viscosity of Al-Na and A0 glasses versus temperature.

The main difference between Al-Na and A0 batches is in the mineral form of the precursor of Al_2O_3. Whereas the Al-Na batch contained corundum, the source of Al_2O_3 in the A0 batch was gibbsite, $Al(OH)_3$. One can reason that $Al(OH)_3$ in the A0 batch released water on heating, leaving behind reactive amorphous oxide that dissolved in the alkali-borate melt. However, corundum took a long time and an increased temperature to dissolve, producing nepheline, $NaAlSiO_4$, as an intermediate crystalline phase [30]. Neither gibbsite nor any other Al-containing mineral was detected in the A0 batch heated to 500°C, whereas the Al-Na batch retained undissolved corundum up to 800°C and contained nepheline at a temperature around 700°C.

The fractions of Al and Si-containing crystalline phases in Al-Na and A0 batches quenched from 700 and 800°C, as measured by XRD, are listed in Table 4. Sodalite-type aluminosilicates were also detected, but are not included in Table 4 because their identification was uncertain. As Table 4 shows, less silica but more alumina were undissolved in the Al-Na melt than in the A0 melt,

9% versus 10% SiO_2 and 6% versus 0% Al_2O_3, both at 700°C. Though these XRD data are semiquantitative and thus subjected to an unknown and possibly large error, the difference in the melting behavior of the Al–Na batch and the A0 batch is beyond doubt.

Table 4 also shows calculated viscosity values at 700 and 800°C for glasses with incompletely dissolved SiO_2 and Al_2O_3 (the matrix glass) as well as for glasses with all components dissolved (final glass). Both SiO_2 and Al_2O_3 impact viscosity more than any other components. The activation energy for viscosity is 1.85×10^4 K for Al–Na glass and 1.84×10^4 K for A0 glass. Removing 1% of SiO_2 decreases the activation energy by nearly 300 K, and removing 1% of Al_2O_3 decreases the activation energy by around 400 K. Whereas the viscosity of glass with all components dissolved (the final glass) was 2.3×10^3 Pa·s for Al-Na and 2.3×10^3 Pa·s for A0, both at 700°C, the average viscosity of Al–Na glass with undissolved SiO_2 and Al_2O_3 dropped to 58 Pa·s at 700°C and that of A0 glass with undissolved SiO_2 decreased only to 460 Pa×s. The lower viscosity caused the initially isolated islands of Al–Na glass-forming melt to connect at a lower temperature, at which the batch gases were still evolving. The higher viscosity of A0 glass-forming melt connected and became continuous at a higher temperature, allowing the final batch gases to escape while the pores were still open.

The viscosity values were obtained for average melt compositions, ignoring the highly nonuniform concentration distribution of melts with dissolving grains. In reality, a fraction of dissolved SiO_2 is stored in the concentration layers around the dissolving particles of solid silica [32]. This means that the bulk melt has a lower fraction of silica than the average shown in Table 4 and thus a lower viscosity. Bubbles easily escape through low-viscosity melt, even if this melt is continuous [32]. As bubbles grow and move through the melt, they increase the degree of melt homogeneity. Therefore, one would expect that delayed dissolution of alumina accelerated quartz dissolution in Al-Na batch. However, as Figure 5 shows, the fraction of undissolved quartz versus temperature was similar for both batches, i.e., Al-Na and A0, even though their foaming behavior was very different.

Figure 6 shows details of the changes in the Al–Na batch morphology with increasing temperature. The batch sintered at 700°C, trapping irregular pores in glass-forming melt that began to connect. The primary-foam bubbles coalesced to larger cavities at 800°C. Bubbles of secondary foam are seen in the sample at 900°C.

Figure 7 displays optical images of thin sections from partly melted A0 batches. The sample heated to the temperature of 800°C formed a melt from the sintered batch containing closed pores. The melt contained residues of silica grains and a large number of small shiny crystals, probably magnetite. At 900°C, secondary foam expanded to a maximum. Tiny crystals of spinel, ~1 mm in size or smaller, were scattered in the glass. Areas with a large number-density of tiny hematite and spinel crystals appeared brown, but microscopic examination revealed that the crystals were embedded in virtually transparent glass (see an optical micrograph of a bubble-free area in Figure 8a).

To check whether spinel crystals were present in the sample before cooling or formed during cooling in air, a 10-g sample of A0 batch was heated in a Pt-crucible to 1200°C at 5°C/min and quenched in water. Figure 8b shows ~1-mm crystals that could only be present in the sample before quenching. To see whether the fraction of crystallinity in the sample was close to equilibrium, another sample was heated at 5°C/min to 1200°C, held at this temperature for 120 min, and then quenched in water. No significant difference in the crystal populations occurred (see Figure 8c). Samples heated to 1200°C were totally free of bubbles.

Table 4. Fractions of quartz, corundum, and nepheline measured by XRD in Al–Na and A0 batch samples heated at 5°C/min to 700 and 800°C and quenched. Also listed are the total undissolved and dissolved fractions of SiO_2 and Al_2O_3 in the glass-forming melt and viscosities based on the average melt compositions.

Temperature	700 °C		800 °C	
Glass	Al–Na	A0	Al–Na	A0
Quartz	0.077	0.099	0.067	0.073
Corundum	0.048		0.008	
Nepheline	0.030			
Undissolved Al_2O_3	0.059		0.008	
Undissolved SiO_2	0.090	0.099	0.067	0.073
Dissolved Al_2O_3	0.155	0.240	0.205	0.240
Dissolved SiO_2	0.256	0.206	0.279	0.232
log(η/Pa·s), matrix glass	1.76	2.66	1.87	2.11
log(η/Pa·s), final glass	3.37	3.32	2.60	2.56

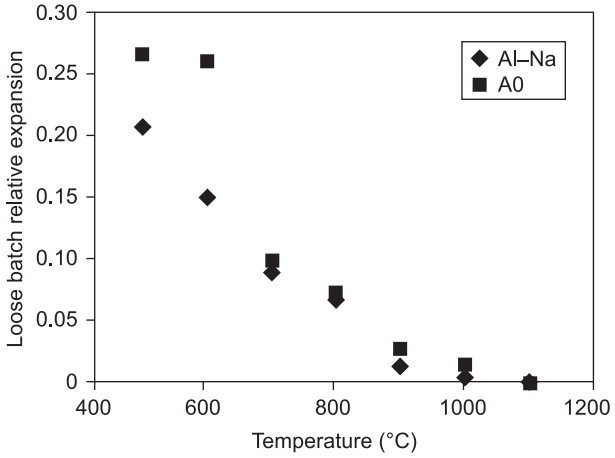

Figure 5. Fraction of undissolved quartz in Al-Na and A0 batches as function of temperature (the heating rate was 5°C/min).

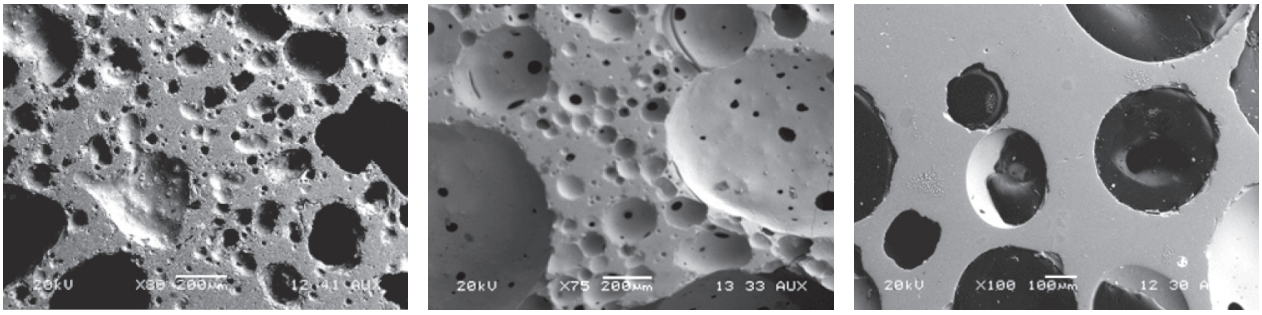

700°C 800°C 900°C

Figure 6. SEM images of sections of Al-Na batches heated at 5°C/min in porcelain crucibles.

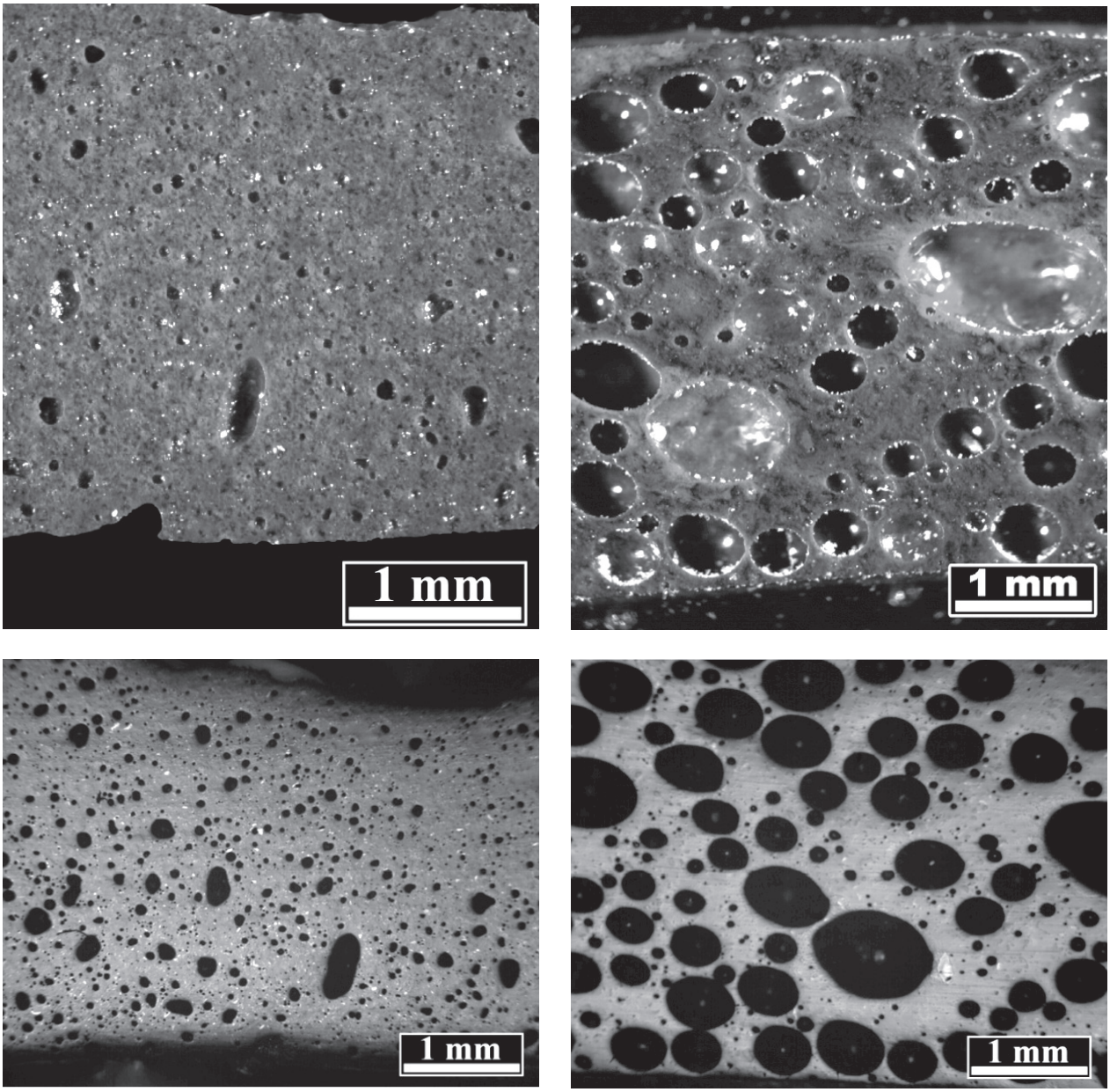

800°C 900°C

Figure 7. Optical images of thin sections of A0 batches heated in Pt crucibles at 5°C/min (top: stereoscope Olympus SZ19; bottom: Olympus PMG3, reflected light).

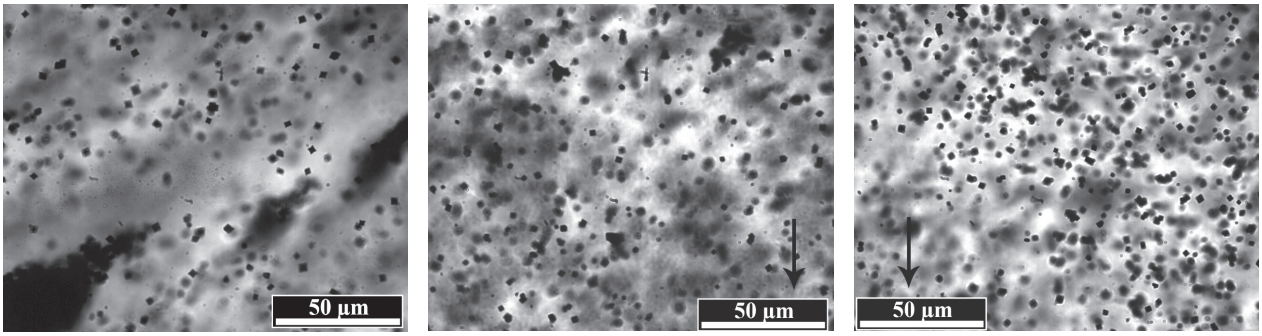

a) b) c)

Figure 8. Optical images (transmitted light) of A0 samples heated at 5°C to 800°C and air-quenched (a), to 1200°C and quenched in water (b), and to 1200°C and quenched in water after a 2-hour dwell (c).

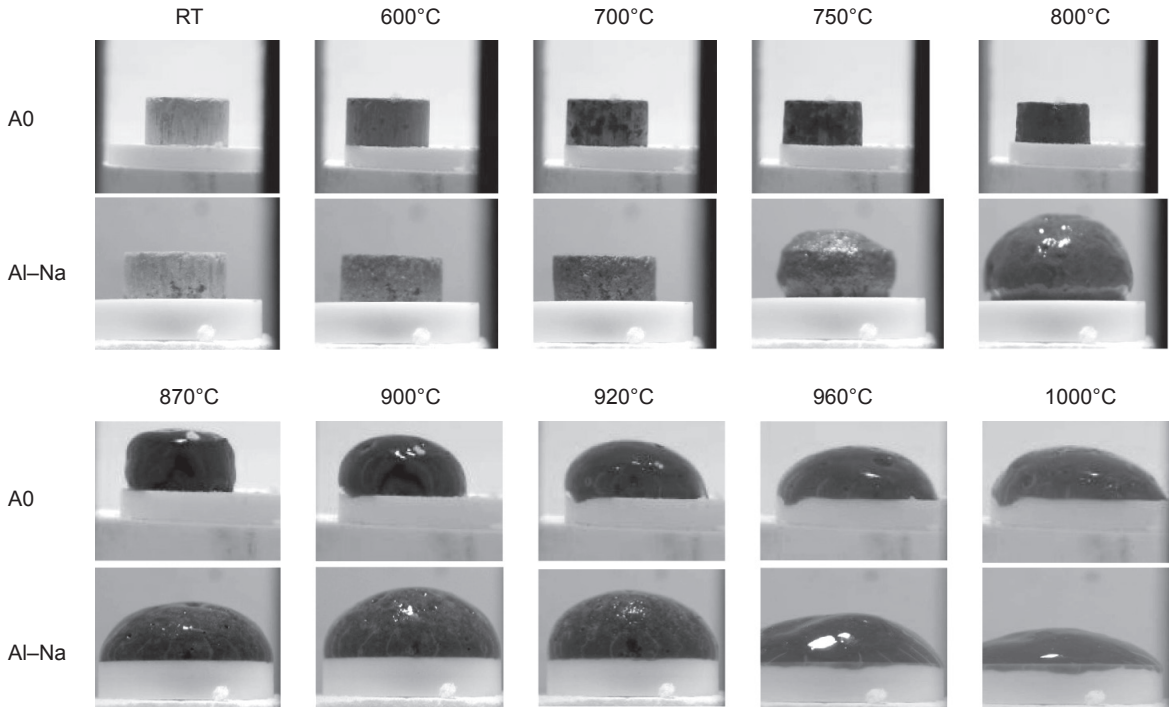

Figure 9. Pellets of A0 and Al–Na batches.

Melting of pellets

Experiments with transparent glass showed that large bubbles can get attached to crucible walls and turn into large stagnant cavities held in place by the high-viscosity melt that formed from the dissolving wall material. These randomly formed cavities were not visible in the opaque batches, and they subjected the measured expansion extent to uncertainty. Since the expansion of pellets, not without other problems (to be discussed below), was free from the wall interference, pellets were made and heat treated to observe batch expansion when crucible walls did not affect the foam development. Figures 9 shows photographs of pellets, and Figure 10 displays the expansion of pellets in

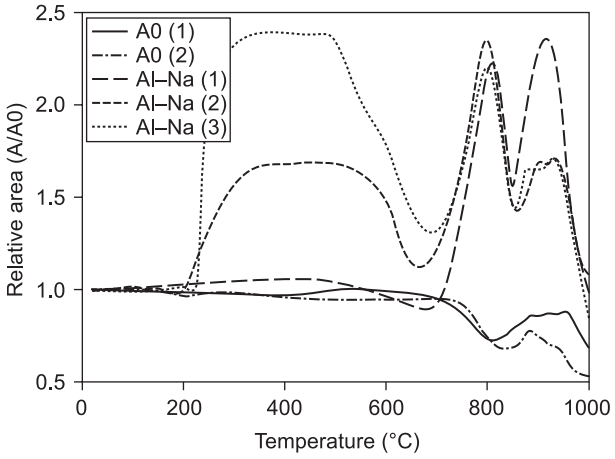

Figure 10. Relative pellet profile area versus temperature for Al–Na and A0 batches heated at 5°C/min.

response to heating at 5°C/min.The relative expansion of pellets was measured as the relative profile area, $a = A/A_0$. The maximum relative expansion of A0 pellets was 0.88. The Al-Na pellet reached maximum expansion at ~815°C and began to collapse to a minimum profile area at ~850°C, after which foam rose again to another maximum at ~920°C (Figure 10). The first maximum is attributable to primary foam, the second to secondary foam. In a commercial glass batch [9, 29], a double peak commonly occurs because the batch expansion temperature and fining temperature are different, but this phenomenon is rare in waste glasses with large fractions of multivalent oxides.

We repeated the experiment to check whether a double peak was not an artifact caused by a large bubble bursting into the atmosphere. No longer having the original slurry, we used the remaining dry Al–Na batch stored for one year in a closed jar. The line marked as Al–Na (2) in Figure 10 represents the result. Surprisingly, a new broad peak appeared on the expansion curve, ranging from 200 to 650°C. The double peak attributed to primary and secondary foam was well reproduced, except that the second peak was milder. At the temperature interval of the broad low-temperature peak, the pellet had a rather rough irregular surface, and the body of the pellet was cracked as seen in Figure 11. We repeated the experiment, this time with a pellet dried for 150 min at 115°C. The result shown as the Al–Na (3) line in Figure 10 is similar to that obtained for the Al–Na (2) pellet, except that the low-temperature peak was even more pronounced, and the pellet shape was even more irregular (Figure 11, right).

The low-temperature expansion of pellets Al–Na (2) and (3) can be rationalized by the following scenario. The low viscosity ionic-salt melt formed initially on the pellet surface and, driven by surface forces, tended to migrate to the "dry" interior. The melt moved with the progressing isotherm to the pellet core where it fused with borate glass-forming melt. This melt expanded as gas bubbles were trapped in it and grew, causing the hard surface to crack. That this scenario occurred in Al–Na (2) and (3) pellets and not in the Al–Na (1) pellet was probably associated with an aging process during the dry-batch storage. The low-temperature expansion did not affect the formation of primary foam.

The relative volume expansion (v) can be obtained from the relative profile-area expansion (a) for a simple geometry of pellet profile. For example, when the initially cylindrical pellet of the radius r_0 and height h_0 becomes a hemispherical body with the radius r, we have $V_0 = \pi r_0^2 h_0$, $A_0 = 2r_0h_0$, $V = (2/3)\pi r^3$, and $A = (1/2)\pi r^2$. Hence, $v_P = 2r^3/(3r_0^2h_0)$, where the subscript P stands for pellet, and $a = \pi r^2/(4r_0h_0)$. Thus, $v_P = (16/3)\pi^{-3/2}(h_0/r_0)^{1/2}a^{3/2} = 0.9578(h_0/r_0)^{1/2}a^{3/2} = 0.754$, where we used the values of $h_0 = 6$ mm, $r_0 = 6.5$ mm, and $a = 0.876$. Repeating this calculation for Al-Na pellets for 900°C expansion values, we obtain for each of the three measurements the v_P values of 3.36, 2.02, and 1.90.

The v_P values are smaller than those for the loose batches, even though the batch in a pellet is compressed to begin with, and thus has a lower initial volume: the loose A0 batch with a density $\rho_C = 0.78$ g/cm^3 was compressed in a pellet to the density of $\rho_P = 1.88$ g/cm^3. Thus, te foam collapse occurs in pellets at a much lower porosity ($p_{max} = 0.45$) than in loose batches placed in silica-glass crucibles. The factors contributing to the differences between loose and compressed batches are pointed out in page 202.

Temperature field evolution and heat conductivity

The temperature-field-evolution for the Al-Na batch is displayed in Figure 12. The horizontal temperature distribution in the batch was close to parabolic at the heating times from 60 to 140 min (when the inner wall temperature was between 200 and 600°C).

The heat flux through the crucible wall was calculated as $q = \lambda_W \Delta T/h$ where λ_W is the heat conductivity of the crucible material, h is the crucible wall thickness, and $\Delta T = T_E - T_I$ is the temperature difference across the crucible wall (T_E and T_I are the temperatures of the external and internal wall surface, respectively). As

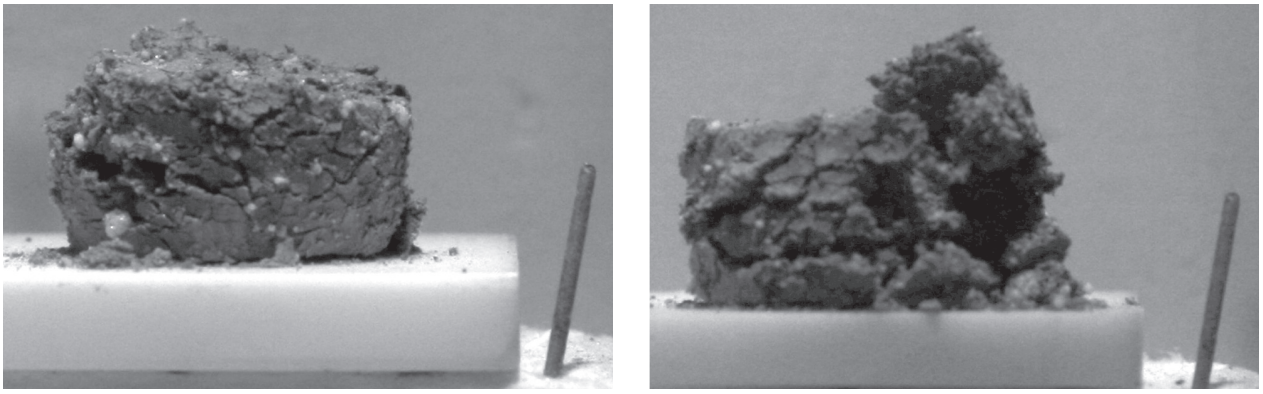

Figure 11. Pellets of Al–Na (2), left, and (3), right, at 450°C. The Pt wire is 10 mm long and is used as a measuring stick.

Figure 12 indicates, a quasi-steady state was established after ~100 min of the experiment and lasted up to ~160 min, when large cavities began to appear in the batch, and the temperature profile turned flat. For the quasi-steady-state interval, the effective heat conductivity (λ_E) of the batch was then estimated as $\lambda_E = q/(dT/dx|_{x=0})$ where x is the horizontal distance from the wall. Table 5 lists the measured and calculated data.

The effective heat conductivity is not a true conductivity because its value is affected by other processes, such as the melting of molten salts and their reactions with batch solids as evidenced by the TGA (Figure 13). The λ_E was probably lower than the true conductivity because the temperature gradient gets steeper if the incoming heat is consumed by batch reactions and phase transitions. In Figure 13, λ_E is plotted versus T. Within 400 and 700°C, the effective heat conductivity of the batch increased as the temperature increased, probably as a result of the increasing batch density.

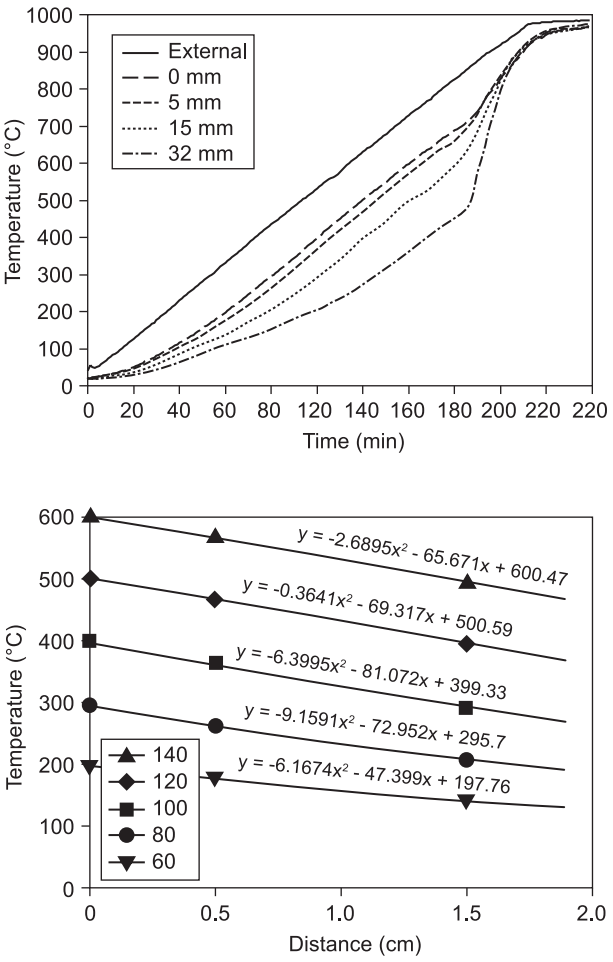

Figure 12. Evolution of temperature distribution within Al-Na batch. Top: Temperature versus time and distance from crucible wall (legend). Bottom: Temperature versus distance from crucible wall and time in min (legend).

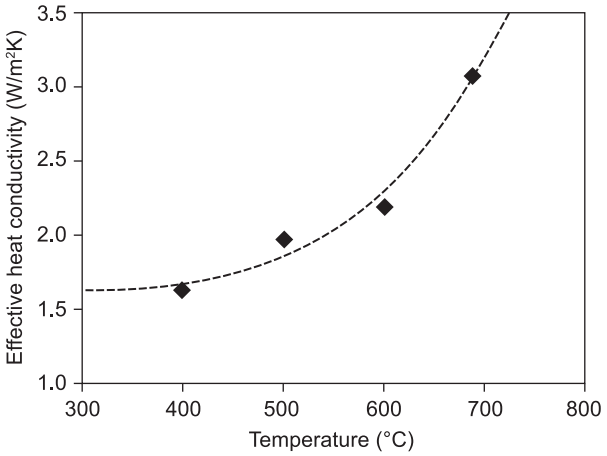

Figure 13. Heat conductivity versus temperature for Al–Na batch.

Effect of silica-grain size on foaming

As Figure 14 demonstrates, batches with 5-mm silica form a large amount of primary foam in A0 batches, while batches with 75-mm and 550-mm silica do not form primary foam at all. Primary foam started in loose batches with 5-mm silica at ~750°C and below 700°C in pellets. The fine (≤5 mm) silica grains react with molten salts forming glass melt below 800°C instead of dissolving in borate melt above 800°C as do ≥75-mm grains. As we have shown elsewhere [32], silica grains larger than 100 mm have a tendency to cluster and

Table 5. Temperature field data*.

Time (min)	T_E (°C)	T_I (°C)	ΔT (K)	$\Delta T/h$ (K/mm)	$-\partial T/\partial x$ (K/mm)	λ_W (W/(m·K))	q (kW/m^2)	λ_E (W/(m·K))
160	826	688	138	10.7	5.32	1.53	16.4	3.1
140	728	600	128	9.9	6.57	1.45	14.4	2.2
120	629	501	129	10.0	6.93	1.37	13.7	2.0
100	532	399	133	10.3	8.11	1.28	13.2	1.6

* T_E is the external wall surface temperature, T_i is the internal wall surface temperatures, $\Delta T = T_E - T_i$, h is the crucible wall thickness, x is the distance from the internal wall surface, λ_W is the heat conductivity of the crucible material, λ_E is the effective heat conductivity of the batch, and q is the heat flux through the crucible wall.

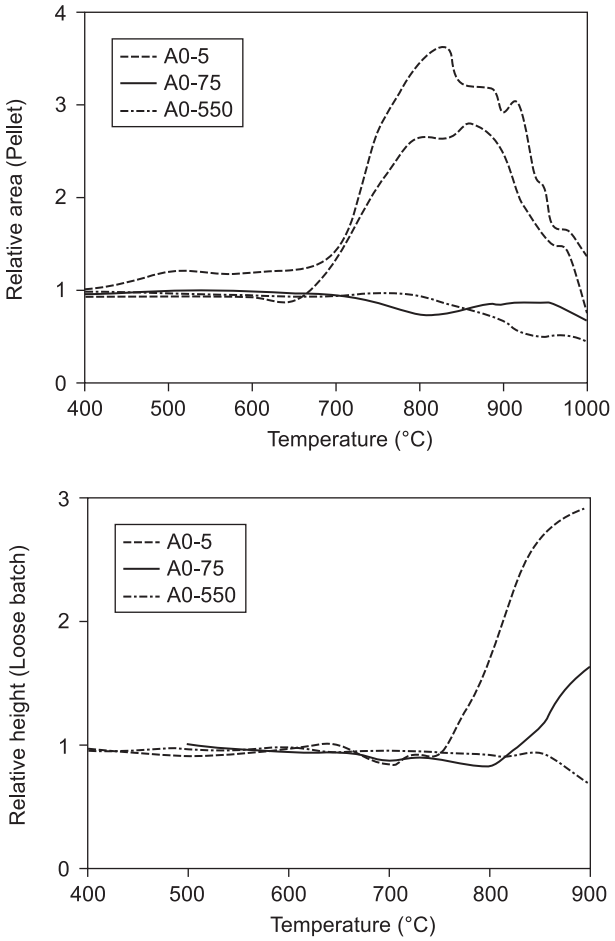

Figure 14. Relative expansion versus temperature for batches with silica-grain sizes 5, 75, and 550 μm (experiment with a pellet containing 5-μm silica was performed twice).

thus slow down melt homogenization.

The stronger foaming of the Al–Na batch was attributed to slowly dissolving alumina that kept the viscosity low, thus allowing the borate melt to close the batch pores more quickly. Contrary to this effect, the early reaction of fine silica with molten salts produces foam because a highly viscous silicate melt forms at T <800°C. In the case of alumina, we have attributed the early foaming to a higher fluidity of glass-forming melt assisted by capillary forces, whereas in the case of silica, the likely cause of the closure of pores is the large fraction of glass-forming melt that becomes continuous through the percolation effect. Indeed, with 5-mm quartz, nearly all batch turns into glass-forming melt while batch gases still evolve.

Effect of sucrose addition to A0 batch

Sucrose was added to the A0 batch after enough HNO_3 was added to it to convert carbonates, hydroxides, and some oxides to nitrates, thus providing oxygen needed for a sufficient internal heat supply. The carbon-nitrogen ratio was C/N = 1. The expansion of this modified A0 batch was nearly the same as that of the original. Pellets of both batches began to expand at ~800°C and reached the maximum volume at ~950°C. Hence, neither made primary foam. The expansion somewhat increased when the A0 batch was acidified without adding sucrose.

Figure 15 displays the temperature field evolution of the modified A0 batch with added HNO_3 and cellulose at C/N = 0.9. The temperature-versus-time curves bring evidence for an exothermic reaction between nitrate and carbohydrate that started at the crucible wall at a temperature 310°C and rapidly propagated towards the center of the crucible, reaching the distance of 35 mm from the wall within a time shorter than 2 min and igniting the reaction there at 160°C. The temperature jump occurred within 1 min and was 200 to 300°C high. The temperature then decreased within 15 to 30 min to a level at which further heating was supplied via conduction. The peak temperature was probably that of the reaction gas from which only a fraction of the reaction heat was transferred to the batch solids.

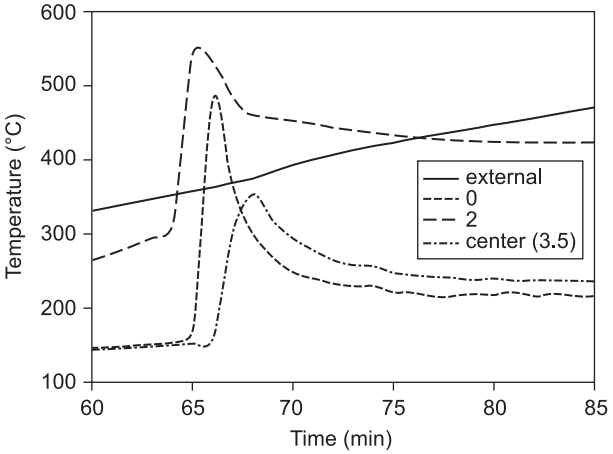

Figure 15. Temperature versus time and distance from crucible wall (legend, in cm) for A0 acidified batch with cellulose (C/N = 0.9).

Effect of composition variation on foaming

The batch expansion data for the composition variation study (A0 to A5 batches) are listed in Tables 6 and 7. Both loose batches and pellets reached minimum volume within the temperature range from 750 to 850°C. The expansion was most rapid around 900°C in loose batches (within the range from 860 to 950°C) and around 850°C in pellets (within the range from 830 to 880°C). The maximum expansion occurred around 980°C (within the range from 950 to 1030°C) in loose batches and around 910°C in pellets (within the range from 870

to 960°C). The average difference between temperatures of maximum and minimum volume was 180°C for loose batches and 110°C for pellets. Assuming that the composition was uniform, foam reached maximum expansion at log(η/Pa·s) = 1.4±0.2 (lose batches) and 1.7±0.1 (pellets). When the value of log(η/Pa·s) for an A5 pellet was removed from the average, the standard deviation decreased to 0.04 Pa·s (corresponding to η = 45±4 Pa·s). The relative maximum expansion was 1.56±0.28 for loose batches and 0.92±0.09 (lower than the initial volume) for pellets.

The maximum rate of expansion (the rate at the inflexion point) was determined by fitting a third-order polynomial to data between the maximum and minimum expansion (not necessarily including these extreme values in the fit). Figure 16 displays measured data for the temperature interval during which expansion occurred. The lines show the third-order polynomials fitted to data.

Figure 17 shows pictures of four pellets arranged by the increasing value of the B/Ca atomic ratio in glass. For the first three (A3, A0, and A1), it was the only composition variable that changed. Figure 18 arranges the pictures of four pellets (A0, A2, A5, and A4) according to the Li_2O mass fraction in glass. Visual inspection indicates that pellets melt faster when the B/Ca ratio increases and when the Li_2O fraction in glass increases.

When applied to the temperature of maximum expansion rate and maximum expansion of pellets, linear regression analysis showed that these temperatures were little affected by the content of CaO, MgO, and Na_2O in glass, but correlated with the content of B_2O_3 and Li_2O. This correlation can be expressed by the equation

$$(T_{\text{inf}}, T_{\text{max}}) = T_0 + T_B x_B + T_L x_L \quad (1)$$

where x_B and x_L are the mass fractions of B_2O_3 and Li_2O, respectively (see Table 3), T_0 is the intercept, and T_B and T_L are the coefficients; Table 8 lists the values. No such correlation was found for T_{inf} and T_{max} of loose batches. One can assume that the foam volume per mass of glass at a characteristic temperature, such as T_{inf}, is a function of temperature and glass composition, i.e.,

$$v = \tilde{v}\,(T_{\text{inf}}, \vec{x}\,) \quad (2)$$

where $\vec{x}$ is the composition vector. Equation (2) can be conveniently linearized as

$$v = v_0 + v_T / T_{\text{inf}} + \sum_{i=1}^{N} v_i x_i \quad (3)$$

where x_i is the i-th component fraction, N is the number of foaming-affecting components, and v_0, v_T, and v_i are constant coefficients.

Experimental determination of these linear coefficients would require a large number of data, and thus would be time and labor consuming. Therefore, the sum of composition terms in Equation (3) is usually replaced by just one term based on the fraction of nonbridging oxygens, basicity, or a similar single characteristic. This simplification ignores the unique and specific effects of individual components but usually provides the expected

Table 6. Expansion parameters for A-series loose batches.

		A0	A1	A2	A3	A4	A5	Average	StDev
	Min	0.83	0.88	0.78	0.75	0.94	0.86	0.84	0.07
V/V_0	Inflection	1.31	1.44	0.98	1.14	1.30	1.13	1.22	0.16
	Max	1.64	1.99	1.19	1.42	1.66	1.40	1.55	0.28
	Min	800	775	748	801	858	831	802	39
T (°C)	Inflection	862	885	885	885	928	918	894	24
	Max	950	960	950	1000	997	1005	977	26
$10^3 \mathrm{d}(h/h_0)/\mathrm{d}T$	Inflection	10.1	8.8	2.8	6.1	7.8	4.64	6.7	2.7
η, Pa·s, at T_{max}	44	40	17	25	10	18	26	14	
log(η/Pa·s) at T_{max}	1.65	1.61	1.24	1.40	0.98	1.25	1.35	0.25	

Table 7. Pellet expansion parameters for A-series batches.

		A0	A1	A2	A3	A4	A5	Average	StDev
	Min	0.68	0.79	0.67	0.62	0.65	0.75	0.69	0.06
A/A_0	Inflection	0.79	0.90	0.77	0.83	0.69	0.82	0.80	0.07
	Max	0.88	1.02	0.88	1.03	0.78	0.93	0.92	0.09
	Min	800	800	755	835	800	800	798	25
T (°C)	Inflection	852	845	826	884	844	845	849	19
	Max	950	940	870	960	870	870	910	44
$10^3 \mathrm{d}(A/A_0)/\mathrm{d}T$	Inflection	2.5	3.4	3.0	6.1	3.1	5.2	3.9	1.4
η, Pa·s, at T_{max}*	44	52	46	40	43	95	45.1	4.3	
log(η/Pa·s) at T_{max}*	1.65	1.71	1.67	1.60	1.64	1.98	1.65	0.04	

* The average and standard deviation do not include A5 data

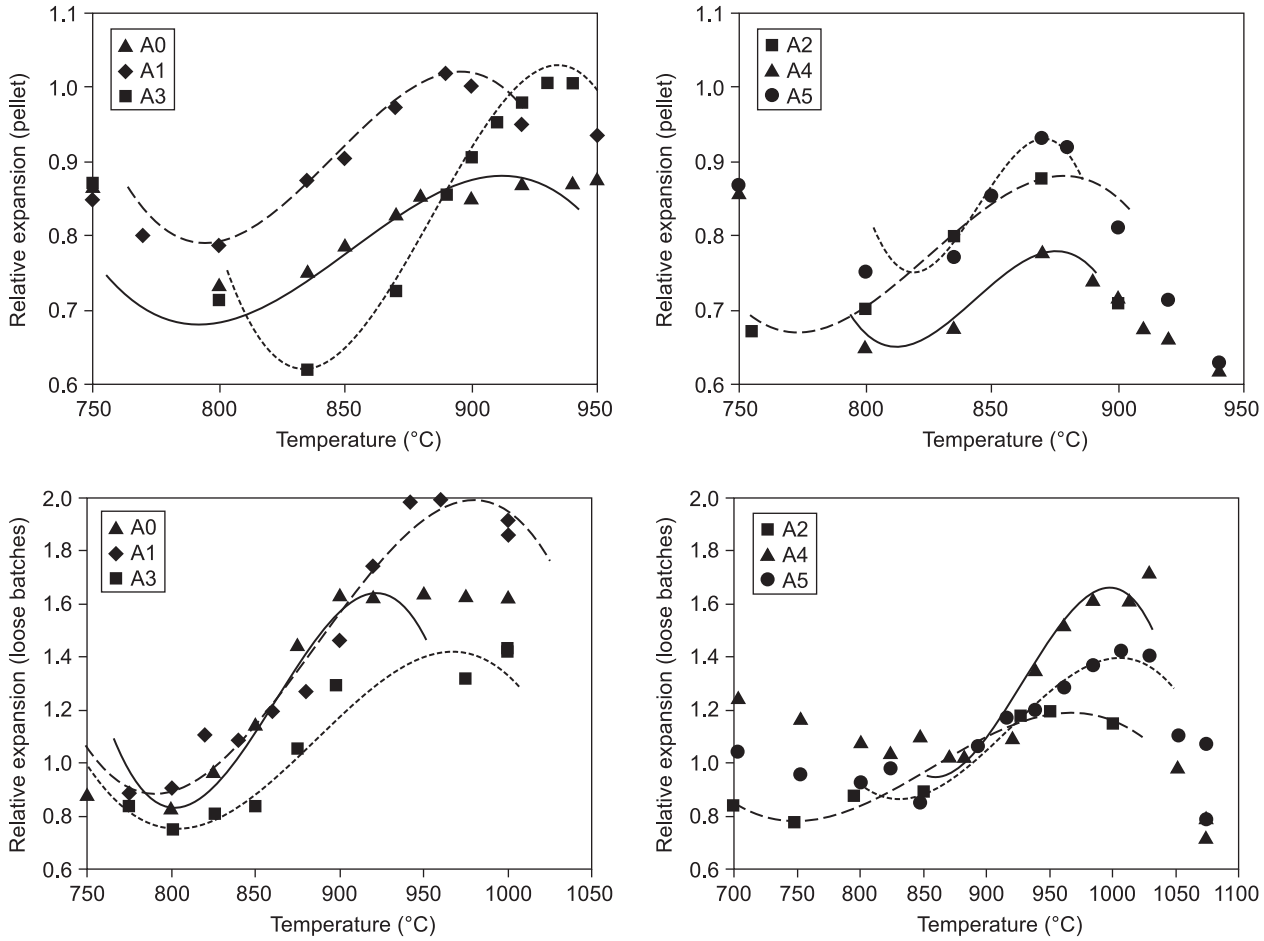

Figure 16. Relative profile areas for pellets (top) and relative volumes of loose batches (bottom) as functions of temperature. The lines represent third-order polynomials fitted to data in the neighborhood of the inflexion point (to assess the maximum expansion rate shown in Tables 6 and 7).

correlation, though with a substantial error.

Foam that evolves at temperatures >800°C is secondary foam from fining-type reactions, such as

$$4Fe^{3+} + 2O^{2-} = 4Fe^{2+} + O_2 \qquad (4)$$

As the temperature increases, the reaction equilibrium shifts to the reduced side of Equation (4); thus, more oxygen is produced, resulting in an increased volume of foam as seen in Figure 19.

Reaction (4) treats Fe(II), Fe(III), and O^{2-} as ions. Though this does not reflect the true nature of iron atoms in molten glass [37], this reaction is nevertheless a useful basis for assumptions that allow estimating the sum term in Equation (3). Various authors [37-41] relate the oxygen activity to the bridging-nonbridging oxygen ratio (more precisely, N_{BO}^2/N_{NBO}, where N_{BO} and N_{NBO} are numbers of bridging and nonbridging oxygens per mole of glass, respectively), or to the optical basicity. Here, following Duffy and Ingram [41], we opted for expressing the influence of glass composition on the redox equilibrium through the optical basicity, Λ, that can be expressed as

$$\Lambda = \sum_{i=1}^{N} \Lambda_i X_i ,$$

where Λ_i is the i-th component coefficient, X_i is the atomic fraction of oxygen per i-th component, and N is the number of components.

Since all iron was initially in the batch in the form of Fe(III), the amount of oxygen evolved via reaction (4) is proportional to the Fe(II) fraction. Because this fraction is small at temperatures £900°C, the volume of oxygen evolved is roughly proportional to the redox ratio, R = [Fe(II)]/[Fe(III)]. A higher melt basicity suppresses the redox ratio according to the relationship [41,42] $\ln(R) = R_0 - R_T/T - R_\Lambda\Lambda$, where R_0, R_T, and R_Λ are positive coefficients.

Figure 20 displays the relative expansions of pellets at three temperatures, T_{min}, T_{inf}, and T_{max} versus basicity calculated for the B_2O_3-CaO-Li_2O-MgO-Na_2O submixture. The Λ_i values of these oxides were 0.40, 1.00, 0.87, 0.87, and 1.11, respectively. These values, recommended by McCloy [43], are somewhat different from those by Duffy [41]. Loose-batch data exhibit a similar tendency as data obtained for pellets, but with a larger scatter. Therefore, we applied linear regression to pellet data rather than loose-batch data using the equation

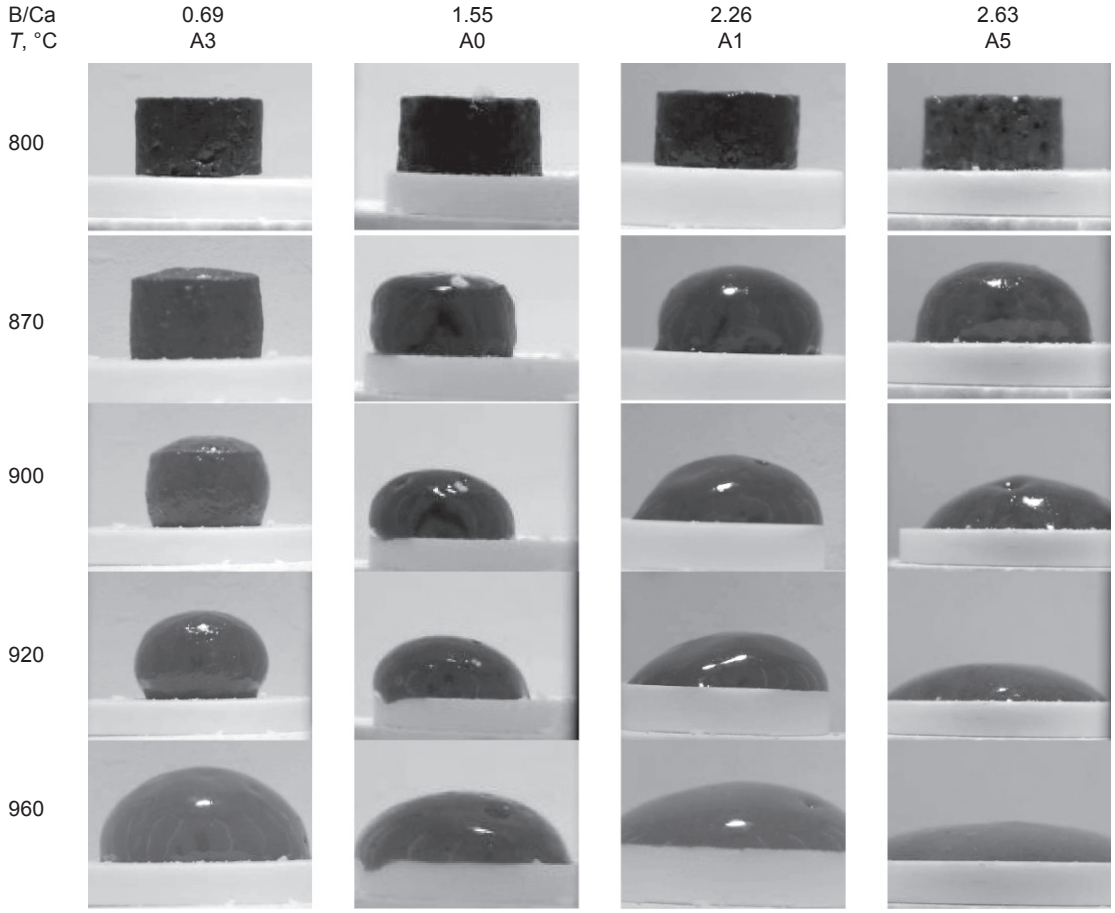

Figure 17. Photographs of selected pellets of A-series batches arranged by B/Ca atomic ratio.

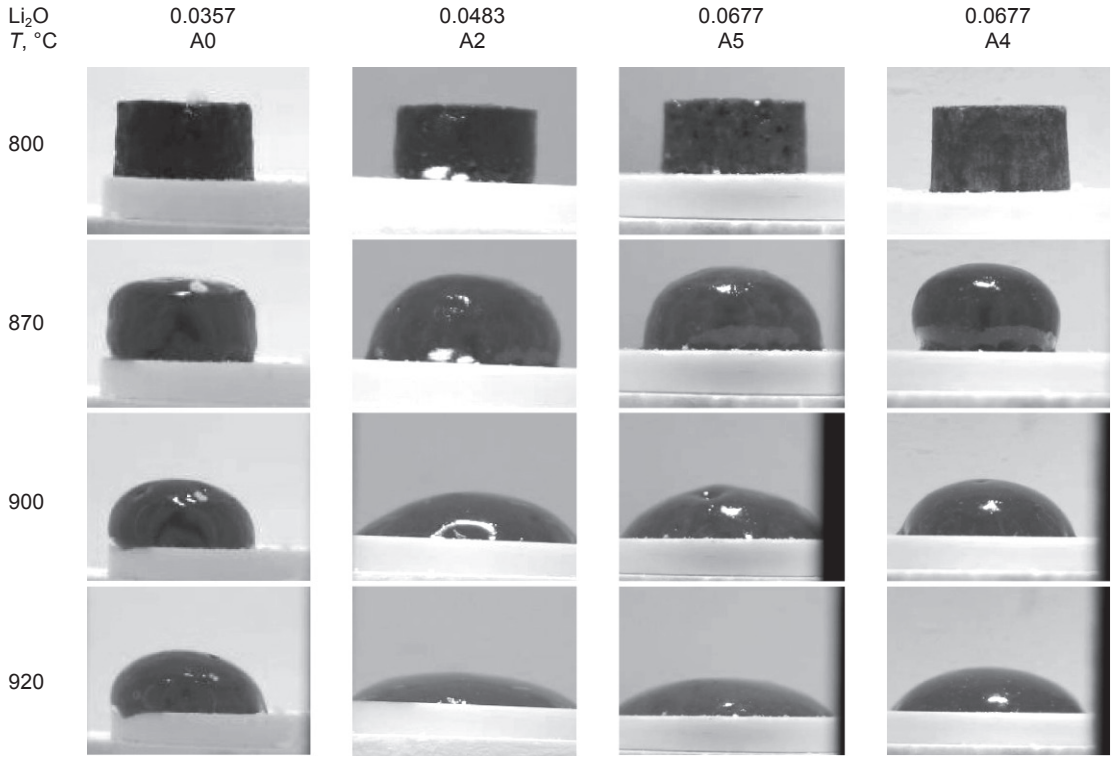

Figure 18. Photographs of selected pellets of A-series batches arranged by Li_2O mass fraction in glass.

Table 8. Coefficients and statistical parameters expressing the effect of B_2O_3 and Li_2O in glass on the temperatures of maximum expansion rate (T_{inf}) and maximum expansion (T_{max}) of pellets (all temperatures are in °C).

	T_0	T_B	T_L	R^2	R^2_{adj}	StError
T_{inf}	992	-678	-954	0.987	0.978	3
T_{max}	1100	-451	-2602	0.826	0.710	24

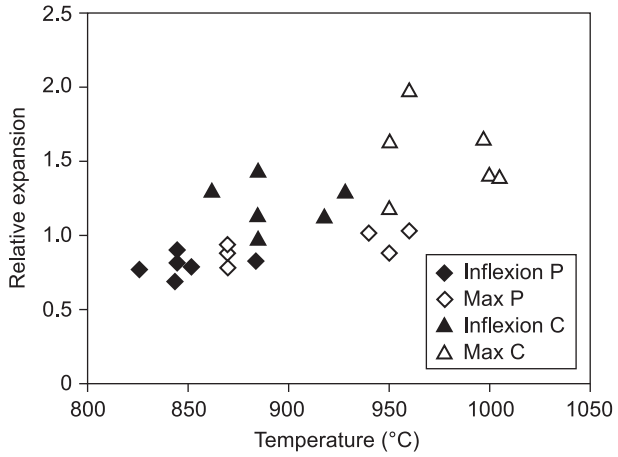

Figure 19. Maximum and inflexion-point relative expansion versus temperature for pellets (P) and loose batches (C).

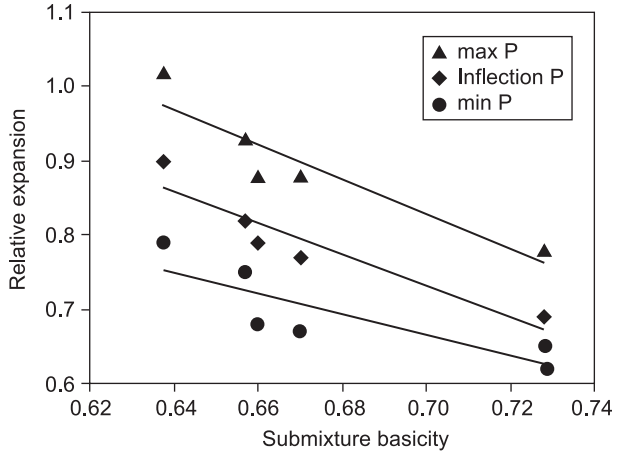

Figure 20. Relative expansion versus B_2O_3–CaO–Li_2O–MgO–Na_2O submixture basicity for pellets (the outlying data points for A3 batch, max and inflexion, were not included in the diagram).

$$a = a_0 - a_T/T - a_\Lambda\Lambda \quad (5)$$

where a_0, a_T, and a_Λ are the coefficients.

As Table 9 and Figure 21 show, the correlation is not perfect. This is owing to various factors unaccounted for: 1) not all oxygen evolved is trapped in secondary foam, 2) foam may contain other gases than oxygen, 3) an unknown portion of the evolved oxygen escapes through the large surfaces of the pellets, 4) residual batch gases, such as H_2O, change the partial pressure of oxygen in bubbles, affecting the extent of foaming and 5) the shape of a pellet is changing with temperature, depending on the surface tension, wetting angle, and the rate of spreading of the melt on the solid surface, and thus its profile area depends of the angle of view. Because of the great sensitivity of foam formation to experimental conditions, the relationship between the batch expansion as observed in the laboratory and the conversion process as it occurs in the batch blanket must be treated with caution (see Discussion). Nevertheless, the existing correlation indicates that the amount of secondary foam in the melter may roughly be estimated based on the redox equilibria as functions of temperature and melt basicity.

Pellets made from the A2, A4, and A5 batches collapsed earlier (at ≤ 960°C) and faster than the high-viscosity pellets A0, A1, and A3. As Table 10 shows, the viscosities of glasses A0, A1, and A3 are virtually identical and higher than those of glasses A2, A4, and A5. This indicates that lower viscosity hastens the foam collapse. Therefore, it also affects the maximum foam volume. This effect is probably responsible for the large error when the maximum foam expansion was expressed as a function of temperature and basicity (Table 9).

Apart from temperature and overall composition, viscosity depends also on the extent to which silica

Table 10. Estimated values of log(η/Pa·s) for A-series glasses (using a mathematical model [35] as functions of temperature. The last column shows measured values for A0 glass for comparison.

T, °C	A4	A2	A5	A0	A3	A1	A0
850	1.75	1.78	2.10	2.23	2.24	2.24	2.29
900	1.47	1.50	1.80	1.93	1.93	1.94	1.96
950	1.21	1.24	1.53	1.65	1.66	1.66	1.66

Table 9. Coefficients and statistical parameters expressing the effect of $1/T$ (for T in K) and B_2O_3–CaO–Li_2O–MgO–Na_2O submixture basicity on the relative expansion of pellets at T_{min}, T_{inf}, T_{max}, and T_{min} with T_{inf}, and at all three temperatures.

	T_{min}	T_{inf}	T_{max}	$T_{min,inf}$	All
a_0	2.88 ±1.03	6.01 ±1.66	2.91 ±1.32	4.07 ±0.57	3.85 ±0.43
a_T, 10^{-3} K	-1.81 ±0.53	-2.05 ±0.63	-0.48 ±1.09	-1.87 ±0.39	-1.43 ±0.41
$a_\wedge$	-1.10 ±0.87	-4.37 ±1.55	-1.99 ±1.27	-2.33 ±0.48	-2.39 ±0.33
R^2	0.80	0.79	0.46	0.79	0.79
R^2_{adj}	0.67	0.66	0.10	0.75	0.76
StError	0.04	0.04	0.09	0.04	0.06

grains dissolved. In Figure 22, the fraction of solid silica is plotted versus temperature for three A-series batches: A0, A1 (yielding glass with the highest viscosity), and A4 (yielding glass with the lowest viscosity). There is little difference between the rates of silica dissolution in these batches, though the data indicate that silica dissolved somewhat earlier in A4 glass. The solid silica was gone by the temperature of 1000°C. Very little or no silica remained in the melt at the temperature interval during which the expansion occurred (800 to 900°C).

Based on the expansion data, one can make three qualitative observations. First, the data scatter is lower for pellets than for loose batches. Second, the slope of expansion versus temperature is milder for pellets. Third, the maximum relative expansion of loose batches is higher and occurs at higher temperatures than that of the pellets. These differences can be attributed to the differences in the heat transfer, the sample sizes, thermocouple placements, and the wall effects. Pellets

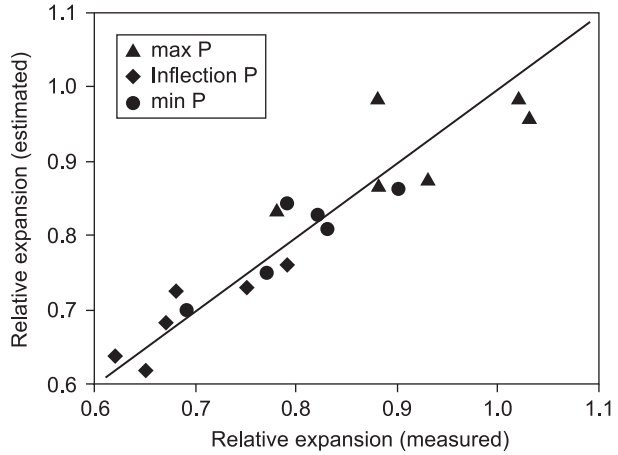

Figure 21. Relative expansion of pellets, estimated versus measured.

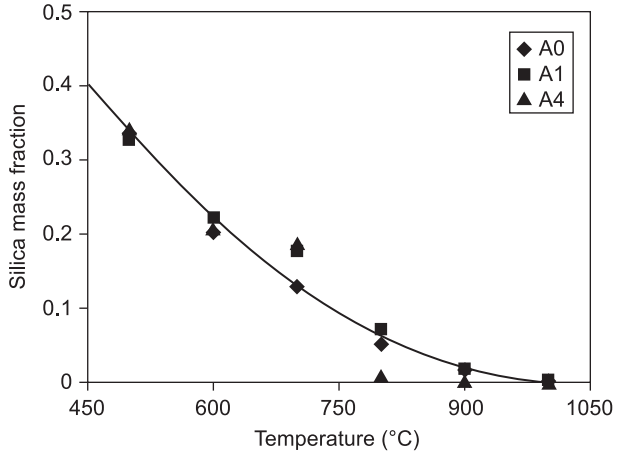

Figure 22. Solid silica mass fraction measured by XRD with RIQAS software of three A-series batches versus temperature (the trendline, $s_U = 1.2055\times10^{-6}$ $(1028.5 - T)^2$, where s_U is the undissolved silica fraction, was fitted using least-square regression).

received direct radiation heat from the heating elements as did the thermocouple. The heating of batch in pellets was close to uniform because of the small volume of pellets and their large surface-to-volume ratio. On the other hand, some of the heat radiation could be reflected back from the silica-glass crucibles while the larger mass of crucible batches and their smaller surface-to-volume ratio lead to a temperature difference between the furnace thermocouple and the batch during the heat treatment at 5°C/min. Also, as already mentioned, batches in crucibles are more subjected to random events, such as growth and collapse of large bubbles hanging on the wall, than batches in pellets with free surfaces.

DISCUSSION

The ultimate goal of batch-melting studies, laboratory-scale, large-scale, or mathematical modeling, is increasing the rate of glass processing in an energy-efficient manner. Each area of study is important in understanding the complexities of melt behavior. Large-scale melter experiments are expensive and time-consuming but are necessary for establishing the actual rate of glass processing and cold-cap formation. For their rational and efficient design, data provided by laboratory batch-melting studies are helpful and necessary. Also, mathematical models are not merely an intermediate step between laboratory-scale and large-scale studies, but also an important tool for processing copious amounts of data and assessing responses of melters to vast combinations of process parameters. This section discusses some aspects of translating experimental data into terms and functions for mathematical modeling.

Non-isothermal crucible tests and melter processing

Translating the batch-conversion process observed during heating batch samples in the laboratory to the conditions at which the batch blanket is converted to molten glass in the melter is a challenging task that can conveniently be accomplished by means of a mathematical model [24]. Such a model would combine the process kinetics with the heat transfer through the low-conductive granular material within the batch blanket and through a layer of primary foam. It also would include the heat exchange between hot reaction gases ascending through the partly molten granular material.

In the simplest continuous steady-state batch melting situation conceivable, a batch blanket of uniform thickness rests on a pool of molten glass from which it receives a steady uniform heat flux [24, 43–46]. The batch is charged from above onto the surface of the batch blanket to maintain its thickness. Ideally, each batch

particle travels vertically down through the blanket, experiencing increasing temperature in response to which its properties change: the density, the dissolution rates of solids, the reaction kinetics, etc. Thus, as the conversion proceeds, the temperature, velocity, and the extent of batch reactions are functions of the position along the vertical coordinate, and these functions do not vary with time.

Although the real melting is accompanied with lateral movements of batch components on various scales, viewing the batch-to-glass conversion as a one-dimensional process is a useful first approximation allowing us to assume that batch conversion reactions advance in a batch blanket in a similar manner as in a crucible heated at the same rate. If the spatial distribution of the temperature can be translated as the temporal history of a small volume of batch in a laboratory crucible, we can expect that the conversion extent translates accordingly.

To approximate conditions a batch particle experiences within the batch blanket, we used a simple temperature history, $T = T_0 + \Phi t$, where T_0 is the initial temperature, t is time, and $\Phi = dT/dt = 5$°C/min is the heating rate. Though this is not the exact duplicate of the melter situation, it is more realistic than the commonly used extremely rapid heating followed by holding the sample at a constant temperature.

Not all conversion phenomena can be reproduced in this manner. Even if the crucible time-temperature function was exactly the same as that in the batch blanket, the conversion process would still be different. The main difference is that a steep temperature gradient exists in the batch blanket in the industrial melter that cannot be easily reproduced in the laboratory situation. Also, gases evolved in the lower layers of the batch blanket rise through the upper layers, exchanging heat and affecting chemical reactions. Further, refluxes of low-viscosity melts [47] that occur in the melter are missing in a small crucible. Techniques have been developed for obtaining more realistic experimental conditions [47–52], but they do not render reliable quantitative data because of problems with melt bridging and other wall effects. Hopefully, a mathematical model will handle these phenomena in their complexity and interrelatedness.

Batch-layer structure

Regardless of the differences discussed above, the time sequence of the conversion stages observed in the crucible informs us about the spatial arrangement in the form of layers in the batch blanket characterized by specific configurations of liquids, solids, and the gaseous phase.

To simplify the situation, we can view a batch blanket as consisting of two main layers that correspond to the two melting stages mentioned in the Introduction: the upper layer of granular solids soaked with low-viscosity molten salts and the lower layer of glass-forming melt containing dispersed solid residues, mainly silica, and, in case of high-level waste glass, spinel, possibly alumina and zirconia, and numerous bubbles. Two conversion stages were identified also by Faber et al. [53] and distinguished by different values of thermal diffusivity. Conradt et al. [54] confirmed their results and argued that measuring electrical conductivity of the batch detects the occurrence of interconnected glass-forming melt whereas thermal diffusivity is influenced by the gas-phase content of the melt after it becomes connected.

Most of the vigorous conversion reactions occur in the upper layer. It is there where the chemically bonded water is released, where oxyionic salts are melting and reacting with organics and solids and where the first borates and silicates form.

If batch solids have a sufficiently large specific surface area, they immobilize the ionic melt via wetting the particles and thus prevent lateral movement of molten salts [33,55]. Then the assumption that the batch blanket melts one-dimensionally is acceptable, at least in the sections of the blanket that are undisturbed by the vent holes through which gases accumulated under the blanket escape (gases that originate from primary foam, from redox and other fining reactions, and from bubblers).

The most important feature that makes the upper layer distinct is that reaction gases can freely escape through the open pores. The volume of gases evolved is impressive. To make 1 g of A0 glass, 1.35 g of batch (Table 2) is needed. The room-temperature volume of gases that this amount of batch evolves during conversion to glass is 17.3 mL (4.3 mL NO, 3.3 mL O_2, 1.6 mL CO_2, and 8.1 mL H_2O), nearly 50 times the volume of glass. At 500°C, this volume increases to 45 mL.

Chemically bonded water (crystalline water and water from hydroxides, oxyhydrates, and boric acid) is liberated simultaneously with the melting of oxyionic salts and the formation of borate melt. The borate melt dissolves amorphous Fe_2O_3 and Al_2O_3 from $Fe(OH)_3$ and $Al(OH)_3$ and reacts with molten salts that react also with organics and with silica. The kinetics of evolution of the borate-melt fraction and its content of R_2O, RO, and R_2O_3 during the reaction progress is largely unknown.

The reaction of nitrates with organics is exothermic and generates a large amount of heat if the concentration of the reactants is high, especially when sucrose is added to a batch containing a large fraction of nitrates [33]. It is unclear what fraction of this heat is used for enhancing the melting process: the rapid escape of hot gases limits the heat exchange with the solid and liquid components. In the case of feeding the melter with water slurry, as is common for nuclear waste batches, evolved gases help evaporate the free water.

To what extent the melting process can substantially

be accelerated through exothermic reactions within the upper layer of the batch blanket depends on how much of the reaction heat produced is lost to offgas.

Obviously, the batch reactions are too numerous to determine their individual kinetics and reaction enthalpies. Fortunately, this is not necessary for designing a mathematical model. Differential scanning calorimetry, TGA, and evolved-gas analysis can provide most of the data needed.

Lower layer of batch blanket and primary foam thickness

In the lower layer of the batch blanket, the borosilicate glass-forming melt is continuous. Gases generated in this layer are trapped as primary foam that collapses when enough gas is evolved to cause the melt films separating the cells to break. Some batches expand several times in volume [23,56].

As has been demonstrated in this study, primary foam can be decreased, and perhaps entirely eliminated, by an appropriate selection of batch additives, especially the size of silica grains. Small silica particles (~5 mm) create a large quantity of a high-viscosity melt too early, leading to massive foaming. On the other hand, silica grains 100 mm in size or larger cannot be recommended because they are sources of inhomogeneities [32]. Also, if glass formulation requires additions of Al_2O_3 or ZrO_2, the mineral form of these components affects the formation of primary foam. This study demonstrated that crystalline Al_2O_3 leads to primary foam generation, whereas $Al(OH)_3$ (gibbsite) does not.

The need to control primary foam can only be based on the knowledge of the impact of primary foam on the rate of melting. This, however, is difficult to assess because it is unclear whether, or to what extent, primary foam hinders heat transfer to the upper portion of the blanket. On the other hand, the formation and collapse of primary-foam bubbles may help dissolve the solid residues and homogenize the melt [14-17].

The thickness (h_P) of the lower layer of the batch blanket in the melter (equal to the thickness of the primary-foam layer if bubbles are present, not to be confused with the secondary foam from bubbles accumulated under the blanket) can be assessed as

$$h_P = \lambda_P \Delta_P T/q \qquad (6)$$

where λ_P is the lower layer heat conductivity, q is the heat flux received from the molten glass under the blanket and $\Delta_P T = T_C - T_{BB}$ with T_C being the temperature at which the glass-forming melt joins into a continuous matrix, and T_{BB} is the batch-blanket bottom temperature.

The heat is produced by the electric energy dissipating in the melt between the electrodes and is delivered to the cold cap by convective currents. For melters without bubbling, the natural convection is driven by buoyancy, and its rate increases as the difference from T_M to T_{BB} increases, where T_M is the melter-operating temperature. Because T_M is limited by the electrode material (it is usually set at 1150°C in nuclear-waste melters), by Equation (6), q decreases as T_{BB} increases. With forced convection by bubblers, the heat transfer greatly improves [57-60].

The batch-blanket bottom is located where the one-dimensional motion of the batch becomes a three-dimensional flow. Thus, the batch-blanket bottom is an important boundary at which the predominantly convective heat transfer from the moving melt turns to a predominantly conductive transfer through the melting batch. The melt-batch interface is positioned where the melt viscosity is low enough to allow the melt to be dragged by the convection currents away from the batch blanket. This viscosity depends on temperature, melt composition, and the fraction of undissolved silica that continues dissolving while carried in the melt-convection currents [61].

Apart from viscosity, the position and temperature of the batch-blanket bottom is influenced by melt density. The bubbly melt under the batch blanket becomes stagnant because its low density blocks convective currents unless the forced convection caused by gas ejected from bubblers blows the bubbly melt away.

The heat flux to the batch blanket is related to the rate of melting (j) as

$$q = jQ \qquad (7)$$

where Q is the total conversion heat per unit mass of glass.

If Q_I is the internal heat supplied by the exothermic reaction that has been transferred from the reaction gases to batch solids and liquids, the rate of melting per heat delivered from electric energy dissipation will increase accordingly, i.e., $j = q/(Q - Q_I)$.

Suppose that $j = 10$ gm^{-2}s^{-1} (0.9 t/m^2/day), $Q = 5$ kJ/g, $Q_I = 0$, and $D_P T = 150$ K. Thus, by Equation (7), $q = 50$ kW/m^2. If the lower layer of the batch blanket consists of bubble-free glass with $\lambda_P = 2$ Wm^{-1} K^{-1}, then, by Equation (6), we obtain $h_P = 6$ mm. The temperature gradient over this layer that is necessary for transferring the conversion heat to the upper layer and maintaining the rate of melting at a constant level would be $\Delta_P T/h_P = 25$ K/mm.

The velocity of the melt is $v = j/\rho_P$, where $\rho_P = \rho_G/(1 - p)$ is the layer density, r_G is the molten glass density and p is the gas-phase fraction (porosity). For $\rho_G = 2.7'10^6$ g/m^3 and $p = 0$, we obtain $v = 13$ mm/h. The time of the passage of melt through the lower layer is $t_P = h_P/v = 27$ min, and the heating rate that the melt experiences is $\Phi = \Delta_P T/t_P = 5.6$ K/min. This is close to the 5°C/min heating rate used in this work.

Repeating the calculation for a bubbly melt, assuming that $p = 0.2$ and $l_P = \lambda$ Wm^{-1}K^{-1}, it follows from the above formulas that $\Phi = j^2 Q(1 - p)/(\lambda_P \rho_G) = 8.9$ K/min. If, on the other hand, λ_P remains at 2 Wm^{-1}K^{-1}, then the

rate of heating would drop to 4.4 K/min. The impact of the gas-phase content on the λ_P is uncertain, especially if bubbles are as large as the foam-layer thickness or when small bubbles move through this layer upwards, dragging hot glass with them.

Would the A0 batch melt faster or slower than the Al-Na batch? Both reach maximum expansion at ~900°C, but the Al-Na batch expanded in a crucible three times as much as the A0 batch (Figure 1). The rate of melting may not be affected by the foaminess of the lower layer of the batch blanket if this layer automatically adjusts its thickness, and thus the temperature gradient, to allow the passage of the heat. However, the presence of foam may cause a decrease of the batch-blanket bottom temperature, thus reducing the heat flux to the blanket. Resolving this issue will need further investigation both in the laboratory and with a mathematical model, and verification with melter experiments.

CONCLUSIONS

Although it is not fully understood at this stage to what extent the decrease or avoidance of primary foam will affect the rate of melting, the present study shows that the choice of batch material and the size of silica grains have a profound impact on the extent of primary foaming and thus identifies the means of control of primary foam formation. Exothermic reactions accelerate heating the batch at an early stage of conversion and thus impact the batch-to-glass conversion kinetics, but do not significantly affect primary foam formation.

The approach developed in this study is a step toward providing data needed for a meaningful and economic design of large-scale experiments aimed at achieving faster melting. This study will provide input for mathematical models of melters that will include the batch blanket as a body with temperature and velocity fields rather than a mere mass source and heat sink with no vertical dimension.

Acknowledgments

Pacific Northwest National Laboratory (PNNL) is operated for the U.S. Department of Energy by Battelle under Contract DE-AC05-76RL01830. The authors are grateful to the U.S. Department of Energy Office of River Protection for financial support. Insightful discussions with Dong-Sang Kim and Albert Kruger helped the authors deepen their understanding of experimental results and the melting process in nuclear waste melters.

References

1. Bickford D. F., Hrma P., Bowen B.W.: J. Am. Ceram. Soc. *73*, 2903 (1990).
2. Hrma P.: Glastech. Ber. *63K*, 360 (1990).
3. Hrma P, Matyáš J., Kim D.-S.: Proc. 9th Biennial Int. Conf. On Nuclear and Hazardous Waste Management, Spectrum '02, American Nuclear Society, CD-ROM, 2002.
4. Gerrard A.H., Smith I.H.: Glastechn. Ber. *56K*, 13 (1983).
5. Blair H. T., Lukacs J.M.: *Investigation of Foaming during Nuclear Defense-Waste Solidification by Electric Melting*, Report PNNL-3552, Richland, Washington, 1980.
6. Bayer G.: J. Non-Cryst. Solids *38*, 855 (1980).
7. Goldman D.S.: , J. Non-Cryst. Solids *84*, 292 (1986).
8. Goldman D. S., Brite D.W., Richey W.C.: J. Am. Ceram. Soc. *69*, 413 (1986).
9. Kim D.-S., Hrma P.: Ceram. Bull. *69*, 1039 (1990).
10. Kim D.-S. Hrma P.: J. Am. Ceram. Soc. *74*, 551 (1991).
11. Preston E., Turner W.E.S.: J. Soc. Glass Technol. *24*, 124 (1940).
12. Hixson A.W., Crowell J.H.: Ind. Eng. Chem. *23*, 923 (1931).
13. Hrma P.: Ceramics-Silikaty *24*, 7 (1980).
14. Hrma P., Barton J., Tolt T.L.: J. Non-Cryst. Solids *84*, 370 (1986).
15. Němec L.: J. Am. Ceram. Soc. *60*, 436 (1977).
16. Mühlbauer M., Němec L.: Am. Ceram. Soc. Bull. *64*, 1471 (1985).
17. Kloužek J., Arkosiová M., Němec L., Cincibusová P.: Glass Technology-European Journal Of Glass Science And Technology Part A *48*, 176 (2007).
18. Savard M. E., and Speyer R.E.: J. Am. Ceram. Soc. *76*, 671 (1993).
19. Sheckler C.A., Dinger D.R.: J. Am. Ceram. Soc. *73*, 24 (1990).
20. Wilburn F. W., Thomasson C.V.: J. Soc. Glass Technol. *42*, 156T (1958).
21. Thomasson C. V., Wilburn F.W.: Phys. Chem. Glasses *1*, 52 (1960).
22. Izak P., Hrma P., Schweiger M.J.: *Kinetics of Conversion of High-Level Waste to Glass*, ACS Symp. Series 778, 314 (2001).
23. Smith P. A., Vienna J.D., Hrma P.: J. Mat. Res. *10*, 2137 (1995).
24. Hrma P.: Glastechn. Ber. *55*, 138 (1982).
25. Hong K. S., Speyer R.E.: J. Am. Ceram. Soc. *76*, 598 (1993).
26. Hong K.S., Lee S.W., Speyer R.E.: J.Am. Ceram. Soc. *76*, 605 (1993).
27. Conroy A. R., Billings D.D., Manring W.H., Bauer W.C.: Glass Ind. *44*, 139 (1963).
28. Manring W.H., Bauer W.C.: Glass Ind. *45*, 354 (1964).
29. Laimböck P.: *Foaming of Glass Melts*, PhD Thesis, Eindhoven University of Technology, 1998.
30. Hrma P., Schweiger M.J. , Arrigoni B.M., Humrickhouse C.J., Mantay V.V., Marcial J., Moody J.A., Rainsdon T.T., Rodriguez C.P., Tate R.M., TeGrotenhuis N.E., Tincher B.H.: *Effect of Melter-Feed-Makeup on Vitrification Process*, Report PNNL-18374, 2009.
31. Hrma P., Schweiger M.J ., Humrickhouse C.J., Moody J.A., Tate R.M., TeGrotenhuis N.E., Arrigoni B.M., Rodriguez C.P.: Proceedings of International Symposium on Radiation Safety Management, p.280, Daejeon, Republic of Korea 2010.
32. Schweiger M. J., Hrma P., Humrickhouse C.J., Marcial J., Riley B.J., TeGrotenhuis N.E.: J. Non/Cryst. Solids *356*, 1359 (2010).
33. Hrma P., Bagaasen L.M., Schweiger M.J., Evans M.B.,

Smith B.T., Arrigoni B.M., Kim D.-S., Rodriguez C.P., Yokuda S.T., Matyas J., Buchmiller W.C., Gallegos A.B., Fluegel A.: *Bulk Vitrification Performance Enhancement: Refractory Lining Protection against Molten Salt Penetration*. PNNL-16773, Pacific Northwest National Laboratory, Richland, Washington, 2007.
34. Vienna J. D., Fluegel A., Kim D.S., Hrma P.: *Glass Property Data and Models for Estimating High-Level Waste Glass Volume*, PNNL-18501, 2009.
35. Hrma P.: J. Non-Cryst. Solids *355*, 257 (2009). See also Czerwinski Z., Szklo i Ceram. *16*, 42, 68, and 158 (1965). (in Polish)
36. Douglas R.W., Nath P., Paul A.: Phys. Chem. Glasses *6*, 216 (1965).
37. Klement R., Kraxner J., Liška M.: Ceramics-Silikáty *53*,180 (2009).
38. Goldman D.S.: J. Am. Ceram. Soc. *66*, 205 (1983).
39. Ottonello G., Moretti R., Marini L., Zuccolini M.V.: Chem. Geol. *174*, 157 (2001).
40. Wiedenroth A., Rüssel C.: J. Non-Cryst. Solids *290*, 41 (2001).
41. Duffy J. A., Ingram M.D.: C. R. Chimie *5*, 797 (2002).
42. Hrma P., Vienna J.D., Wilson B.K., Plaisted T.J., Heald S.M.: J. Non-Cryst. Solids *352*, 2114 (2006).
43. McCloy J.S.: paper in preparation.
44. Kuhn W. S.: *Mathematical Modeling of Batch Melting*, in: Loch H., Krause D. (Editors), Mathematical Simulation in Glass Technology, Springer, Berlin Heidelberg, 2002.
45. Ungan A., Viskanta R.: Glastechn. Ber. *59*, 179 (1986).
46. Hrma P. in: Adv. in Fusion of Glass, 10.1, Amer. Ceram. Soc., Westerville, Ohio, 1988.
47. Hayes J.G. in: Adv. in Fusion of Glass, 13.1, Amer. Ceram. Soc., Westerville, Ohio, 1988.
48. Kim D.-S., Hrma P.: Ceram. Trans. *45*, 40 (1994).
49. Elliott M. L., Chapman C.C., Eyler L.L., Yasuda D.D.: *Preliminary Studies of Vitrification Rate Enhancement.* Pacific Northwest Laboratory, Richland, Washington.1989.
50. Josephs J.E., Stone M.E.: *Melt Rate Improvement for DWPF MB3: Sugar Addition Test*. WSRC-TR-2001-00158, Westinghouse Savannah River Company, Aiken, South Carolina, 2001.
51. Lambert D. P., Lorier T.H., Peeler D.K., Stone M.E.: *Melt Rate Improvement for DWPF MB3: Summary and Recommendations*. WSRC-TR-2001-00148, Westinghouse Savannah River Company, Aiken, South Carolina, 2001.
52. Smith M.E., Miller D.H., Lorier T.H.: *Impact of Batch Preparation Acid Stoichiometry and Redox on Melt Rate for the SB3-Frit 418 Batch System*. WSRC-TR2004-00350, Savannah River National Laboratory, Aiken, South Carolina, 2004.
53. Faber A. J., Beerkens R.G.C., de Waal H.: Glastechn. Ber. *65*, 177 (1992).
54. Conradt R., Suwannathada P., Pinkhaokham P.: Glastechn. Ber. *67*, 103 (1994).
55. Hrma P., Goles C.E., Yasuda D.D.: Ceram. Trans. *23*, 361 (1991).
56. Darab J.G., Meiers E.M., Smith P.A.: Mat. Res. Soc. Proc. *556*, 215 (1999).
57. Němec L.: Sklar a Keramik *29*, 103 (1979). (in Czech)
58. Pchelyakov K.A. : Glass Ceram. *28*, 402 (1971).
59. Ungan A., Viskanta R.: J. Am. Ceram. Soc. *69*, 382 (1986).
60. Ungan A.: Glastechn. Ber. *60*, 71, 115 (1987).
61. Němec L., Cincibusová P.: Ceramic-Silikáty *53*, 145 (2009).